ARTICLE NO. 79-1562R

J80-174

Measurements and Axisymmetric Model of Spatial Correlations in Turbulent Pipe Flow

20010
20016
20019

Y. A. Hassan,* B. G. Jones,† and R. J. Adrian‡
University of Illinois at Urbana-Champaign, Urbana, Ill.

The structure of fully developed turbulent water pipe flow is investigated using data from two hot film x probes to evaluate two-point, two-component (axial and radial) space and space-time velocity correlations. Measurements are made with one probe fixed at $Y/R=0.35$ from the pipe wall and the other a moveable probe translated, with combined axial and radial separations, to give net probe separations in planes inclined at 0, 10, 20, 40, 65, and 90 deg in both upstream and downstream directions with respect to the mean flow. Departure of these two-point correlations from isotropic behavior is modeled in terms of axisymmetric tensor forms in which the turbulence is characterized by two scalar quantities related to the correlation length scales.

I. Introduction

SPATIAL and space-time correlations have been used extensively in the study of turbulent flow structure by many investigators. Spatial correlations were initially measured by Favre et al.[1,2] in turbulent boundary layers; Davies and Fisher[3] in the turbulent mixing region of a jet; and Sabot and Comte-Bellot[4] in fully developed air pipe flow, to list only a few. The deduction of the general form of turbulent structure from space-time correlation measurements is also of interest. These measurements have revealed that the major axis of the isocorrelation contours of the convected turbulent structure is inclined to the wall.[5] A positive time delay of the signal from the downstream probe is observed for the maximum correlation coefficient for axial separation, and the time delay increases as the separation increases.

The departure of the two-point correlations from isotropic behavior has demonstrated the need to improve the modeling of second-order velocity covariances beyond the symmetric structure imposed in isotropic models. Additionally, asymmetric structure with respect to time delay in space-time correlations has been observed as well as differences in intensities for the velocity components and nonzero shear correlation coefficients.

In an attempt to model more appropriately second-order velocity covariance structure in shear flows, Batchelor[6] introduced and Chandrasekhar[7] extended the use of axisymmetric tensor forms for these covariances. Unlike the isotropic model, in which time averages of velocity components and their space and time derivatives are invariant under arbitrary rotations and reflections with respect to the reference axes, the axisymmetric model of these time averages is invariant, not for the full rotation group, but for a preferred direction for rotation and certain related planes for reflection.

Herring[8] investigated the approach of axisymmetric turbulence to isotropy using the direct interaction approximation. In his formalism the correlation matrix was represented in terms of its eigenmodes. Sreenivasan and Narasimha[9] expressed the two independent scalar functions that describe the axisymmetric spectral tensor in terms of the Fourier coefficients of an expansion in zonal harmonics, while Herring[8] used an expansion in spherical harmonics for these quantities. In this study the forms of the two scalar functions are postulated to give correlation contours which compare well with experimental measurements.

The present experimental investigation was carried out in a liquid turbulent pipe flow at a Reynolds number of 60,000 based upon the mean flow velocity. The measurements were made in water using two hot film x probes, one fixed at reference point 0, located at $Y/R=0.35$ from the pipe wall, and the other a movable one translated, with combined axial and radial separations, to give net probe separations in planes inclined at 0, 10, 20, 40, 65, and 90 deg with respect to both the downstream and upstream mean flow directions, as shown in Fig. 1. Emphasis was placed on obtaining space and space-time correlations from which to construct isocorrelation contour curves.

II. Experiment

Experimental Facility

The facility in which this study was conducted was a closed recirculating water loop with a 10.16-cm-diam, 9.15-m-long circular vertical test section. All measurements were taken 80 diameters from the highly contracted, smooth nozzle entrance to the test section, thus providing fully developed conditions at the measurement points. The characteristics of both the experimental loop and the test section have been discussed in detail by Burchill.[10] The system water was demineralized to allow the use of uncoated hot film sensors. The specific conductivity of the water was maintained below 1 μmho/cm by bypassing a small flow through a mixed bed demineralizer. The demineralization requirements were minimized by constructing the entire loop of stainless steel. The loop water temperature was kept constant at 27°C with a deviation on any set of runs less than ±0.1°C to avoid the need for anemometer overheat ratio corrections to be applied in velocity measurements.

A traversing mechanism, designed to enter the test section from the top, allowed both radial and axial probe positioning. Two end flow x probes, with 0.0051 cm diameter and 0.1 cm active length sensors, were used to measure the axial and radial fluctuating velocity components. The stationary x probe was located at reference point 0 at $Y/R=0.35$ from the wall as indicated in Fig. 1. At this reference point, corresponding to $y^+=427$, the mean velocity was 0.55 m/s;

Received July 18, 1979; presented as Paper 79-1562 at the AIAA 12th Fluid and Plasma Dynamics Conference, Williamsburg, Va., July 23-25, 1979; revision received Nov. 29, 1979. Copyright © 1979 by B. G. Jones. Published by the American Institute of Aeronautics and Astronautics, Inc., with permission.

Index categories: Nozzle and Channel Flow; Viscous Nonboundary-Layer Flows; Subsonic Flow.

*Research Assistant, Nuclear Engineering Program.

†Professor of Nuclear and of Mechanical Engineering. Member AIAA.

‡Associate Professor of Theoretical and Applied Mechanics and of Nuclear Engineering.

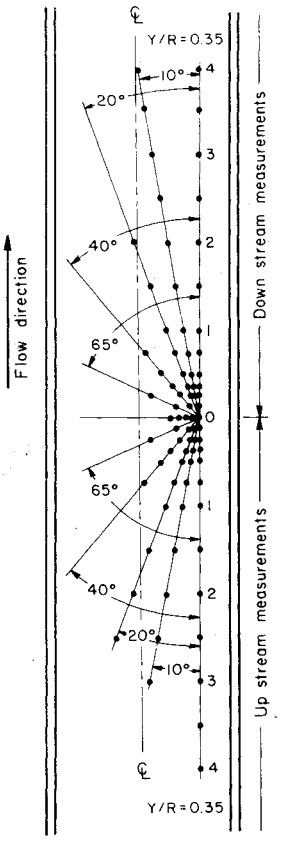

Fig. 1 Spatial separation grid used for correlation measurements; fixed x probe is located at point 0.

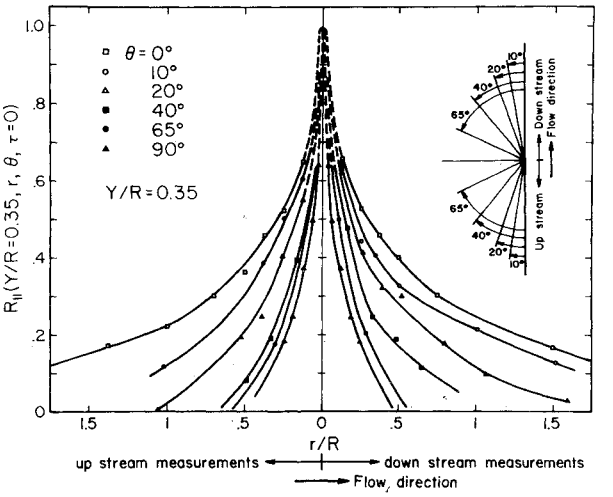

Fig. 2 Spatial correlations, axial velocity components.

the rms of the longitudinal and transverse turbulent velocity components were $u_1' = 0.027$ m/s and $u_2' = 0.019$ m/s, respectively, and the correlation coefficient was $\overline{u_1 u_2} / u_1' u_2' = -0.43$.

Instrumentation

The two x probes were used in conjunction with four channels of anemometry, each consisting of one DISA 55D01 constant temperature anemometer, one DISA 55D10 linearizer, and one dc amplifier with -24 dB/octave low pass filter using a cutoff frequency of 1 kHz. TSI Model 1015C correlators with high pass cutoff frequencies set at 0.1 Hz were used for ac coupling. The four band-passed filtered signals were recorded on FM tape for subsequent data processing. At the beginning of each test run the voltage of each anemometer was calibrated against flow velocity, and the resulting calibrations were used to select the best exponent for anemometer linearization. Because the turbulence intensity levels were low (less than 5%), the yaw response was represented adequately by the cosine law.

The u_1 and u_2 velocity components for each probe were obtained from the recorded x probe signals using two TSI 1015C sum and difference correlators. Auto-covariances and cross-covariances, as a function of time delay, were measured with a Honeywell-Saicor Model 42 100-point digital correlation and probability analyzer using precomputation delay to obtain 400 point covariances.

To check the accuracy of the covariance results, three additional independent sets of instruments and determinations were used. The zero time lag covariance value was employed to check the amplitude of the results and was obtained using: a TSI 1015C correlator in conjunction with a TSI 1060 true rms voltmeter, a Nicollet SD-75A 1000-point digital correlator, and direct digitization of the signals by a Nicollet SD-72/4A analog-to-digital converter, followed by FFT analysis in a digital computer. These results all agreed to within 4%. The functional shape of the covariances, with respect to time delay and both with and without spatial separation, as obtained by the latter two checking procedures, also agreed well with the primary determinations.

Experimental Results: Auto- and Cross-Correlations

Cross-covariances were obtained for 80 different separations and were normalized by the zero time lag values to give the normalized cross-correlation coefficients.

The cross-correlations of the velocity components u_i and u_j with $i = 1, 2$ and $j = 1, 2$ and between the stationary probe (0,0) and movable one (r_1, r_2) are defined by

$$R_{ij}\left(\frac{Y}{R}, r_1, r_2, \tau\right) = \frac{\overline{u_i(0,0,t)\, u_j(r_1, r_2, t+\tau)}}{\sqrt{\overline{u_i^2(0,0,t)}}\sqrt{\overline{u_j^2(r_1, r_2, t)}}} \tag{1}$$

where an overbar indicates a time average, τ is the delay time between the signals from the two probes, and r_1 and r_2 are the Cartesian components of the two-dimensional separation vector r located in the x-y plane. When expressed in terms of the radial separation r and the angle θ the cross-correlation coefficient is defined by

$$R_{ij}\left(\frac{Y}{R}, r, \theta, \tau\right) = \frac{\overline{u_i(0,0,t)\, u_j(r, \theta, t+\tau)}}{\sqrt{\overline{u_i^2(0,0,t)}}\sqrt{\overline{u_j^2(r, \theta, t)}}} \tag{2}$$

where u_i and u_j continue to represent the components in the x and y directions, respectively.

Cross-correlations without time delay ($\tau = 0$) are plotted in Figs. 2-5 vs the radial separation r for different angles θ with different combinations of the axial and radial velocity components for downstream and upstream measurements. Dashed lines indicate extrapolations to the zero separation values determined from single probe data by applying Taylor's hypothesis.

In terms of r and θ an integral length scale, L_{ij}^{θ}, has been defined as

$$L_{ij}^{\theta} = \int_0^{\infty} R_{ij}\left(\frac{Y}{R}, r, \theta, \tau = 0\right) dr \tag{3}$$

When R_{ij} contained negative lobes, the upper limit of integration was taken as the position of its first zero crossing.

The integral scales L_{11}^{θ}, L_{12}^{θ}, L_{21}^{θ}, and L_{22}^{θ} for different angles θ are shown in Table 1. Accuracies of these length scales are estimated to be better than 10%. It is found that the relation $L_{11}^{\theta} > L_{21}^{\theta} > L_{12}^{\theta} > L_{22}^{\theta}$ holds for θ between 0 and 10 deg. This changes to $L_{11}^{\theta} > L_{22}^{\theta} > L_{21}^{\theta} > L_{12}^{\theta}$ as θ increases to 90 deg. The transition occurs gradually around $\theta \sim 30$ deg. This value is roughly equal to a turbulent shear angle β of 25 deg at

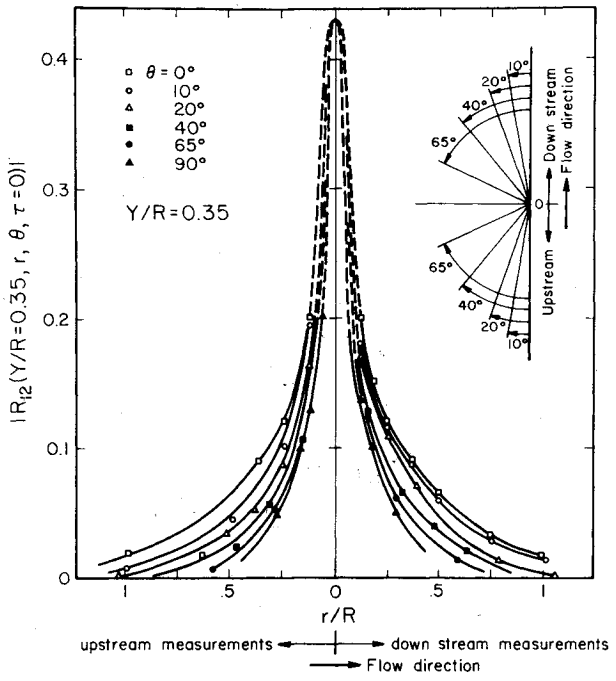

Fig. 3 Spatial correlations, axial and radial velocity components.

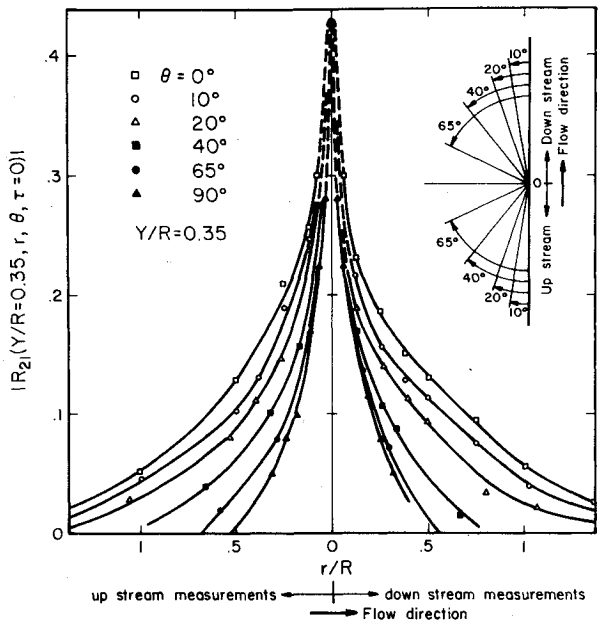

Fig. 4 Spatial correlations, radial and axial velocity components.

this position where

$$\beta = \frac{1}{2}\tan^{-1}\left(\frac{2\overline{u_1 u_2}}{u_1'^2 - u_2'^2}\right)$$

Isocorrelation contours of R_{11}, R_{12}, R_{21}, and R_{22} at $Y/R=0.35$, $\tau=0$ have been obtained. The results for R_{11} are shown in Fig. 6 as an example. The curves are typically tilted oval shapes and they are qualitatively similar to those found in air pipe flow by Sabot and Comte-Bellot,[4] and in homogeneous shear flow by Favre[11] and by Champagne, Harris, and Corrsin.[12] The major axis is tilted about 3-5 deg to the direction of the mean flow.

Figure 7 shows the isocorrelation contours of R_{22} which are much less elongated and more nearly circular than the R_{11} contours. It appears that the spatial extent of coherent radial

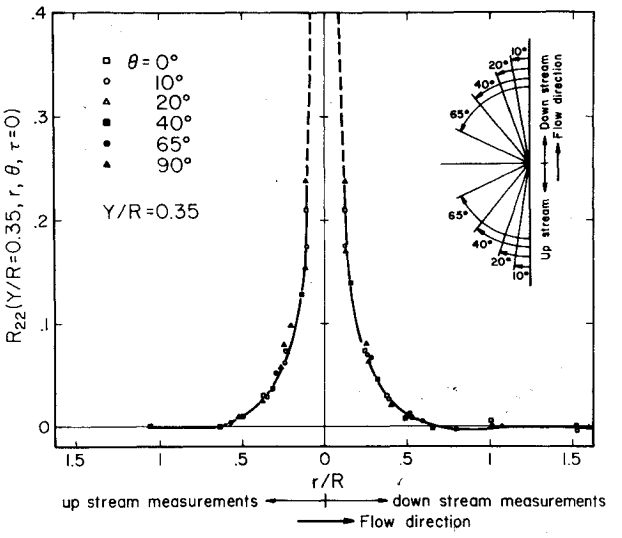

Fig. 5 Spatial correlations, radial velocity components.

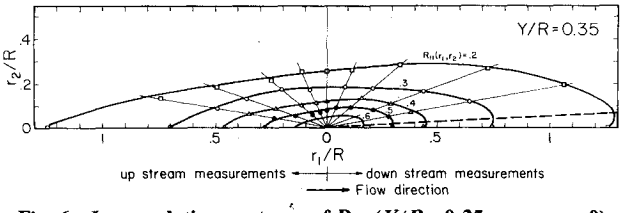

Fig. 6 Isocorrelation contours of R_{11} ($Y/R=0.35, r_1, r_2, \tau=0$).

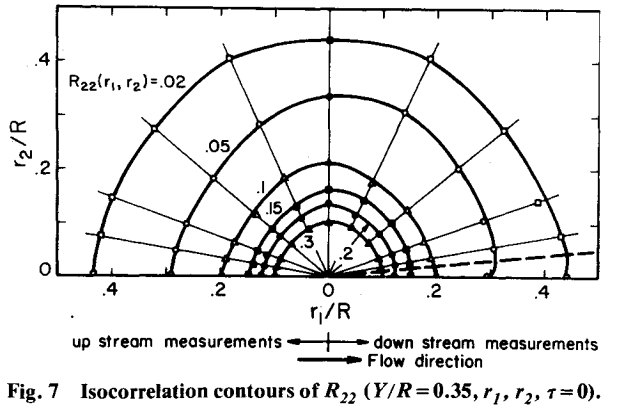

Fig. 7 Isocorrelation contours of R_{22} ($Y/R=0.35, r_1, r_2, \tau=0$).

velocity fluctuations is much less than the scale of axial velocity fluctuations.

The space-time correlations with axial separation, $R_{ij}(Y/R=0.35,\ r_1,r_2=0,\tau)$, and radial separation, $R_{ij}(Y/R=0.35,\ r_1=0,r_2,\tau)$, have been measured for $(i,j)=(1,1)$, $(1,2)$, $(2,1)$, and $(2,2)$. In addition $R_{11}(Y/R=0.35, r,\theta,\tau)$ has been measured for $\theta=10$, 20, 40, and 65 deg. Figure 8 shows the results for $R_{22}(Y/R=0.35, r_1,r_2=0,\tau)$.

The local turbulent convection velocity, found from the locations of the correlation maxima, is $U_c=0.97\,\bar{U}$.

Integral time scales in a coordinate frame moving at the convection velocity T_{ij} were also evaluated from a best fit of a simple exponential function, giving $T_{11}=645$ ms and $T_{22}=140$ ms. The slow rate of change of the correlations with large axial separations suggests the emergence of a preferred turbulence structure as also found by Mulhearn and Luxton.[13]

Probe interference effects for small axial separations were evaluated by comparing autocorrelations with time delay to autocorrelations with axial spatial separation assuming

Table 1 Integral length scales L_{ij}^{θ} (in cm) for selected angles of inclination to mean flow, θ

θ deg	L_{11}^{θ}	L_{22}^{θ}	L_{12}^{θ}	L_{21}^{θ}	
0	2.98	0.42	0.54	1.16	$L_{11}>L_{21}>L_{12}>L_{22}$
10	2.17	0.42	0.46	0.79	$L_{11}>L_{21}>L_{12}>L_{22}$
20	1.50	0.42	0.39	0.68	$L_{11}>L_{21}>L_{22}>L_{12}$
40	0.95	0.42	0.33	0.39	$L_{11}>L_{22}>L_{21}>L_{12}$
65	0.83	0.42	0.28	0.30	$L_{11}>L_{22}>L_{21}>L_{12}$
90	0.68	0.42	0.26	0.29	$L_{11}>L_{22}>L_{21}>L_{12}$

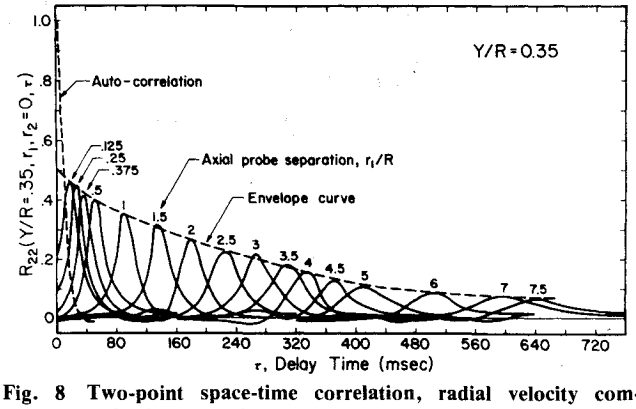

Fig. 8 Two-point space-time correlation, radial velocity components, and axial separations.

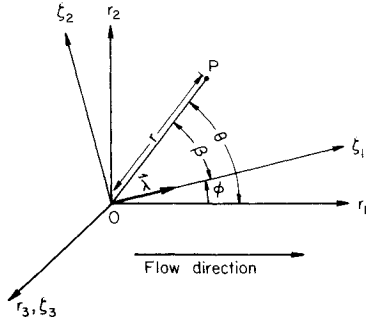

Fig. 9 Systems of coordinates: (r_1,r_2,r_3) measurement system and (ξ_1,ξ_2,ξ_3) axisymmetric system.

Taylor's hypothesis to be correct for small separations. It was found that R_{11} and R_{22} correlation curves obtained with spatial separation could be up to 10 and 30% less, respectively, than those using time delay for $r_1/R<0.4$.

III. Theory

Formalism of Axisymmetric Turbulence Model

For axisymmetric turbulence theory, the two-point covariance tensor defined by

$$Q_{ij}=\overline{u_i(x)u_j(x+r)} \tag{4}$$

is invariant for rotations about a preferred axis with direction λ and for reflections in planes containing this axis. This theory, as in isotropic turbulence, assumes local homogeneity which makes it applicable only to regions in the flowfield where the length scales are small relative to the spatial variation of turbulence intensities.

The general second-order tensor considered by Batchelor[14] is of the form

$$Q_{ij}=A\xi_i\xi_j+B\delta_{ij}+C\lambda_i\lambda_j+D\lambda_i\xi_j+E\xi_i\lambda_j \tag{5}$$

in which ξ_1 is chosen to be in the λ direction and ξ_3 to coincide with x_3 as in Fig. 9. A tilde ($\tilde{}$) over a letter is used to denote the components of vectors and tensors referred to the axisymmetric coordinate system. A, B, C, D, and E are arbitrary scalar functions of $r^2(=\xi_i\xi_i)$ and $\mu r(=\xi_i\lambda_i)$. Since the flow is locally homogeneous and incompressible, it follows from the continuity equations that $\tilde{Q}_{ij}$ is solenoidal:

$$\frac{\partial\tilde{Q}_{ij}}{\partial\xi_i}=\frac{\partial\tilde{Q}_{ij}}{\partial\xi_j}=0 \tag{6}$$

Thus, $D=E$ and Eq. (5) becomes

$$\tilde{Q}_{ij}=A\xi_i\xi_j+B\delta_{ij}+C\lambda_i\lambda_j+D(\lambda_i\xi_j+\xi_i\lambda_j) \tag{7}$$

As a result of this solenoidal property, Chandrasekhar[7] has expressed $\tilde{Q}_{ij}$ in terms of the skew axisymmetric tensor, $\tilde{q}_{ij}$,

$$\tilde{q}_{ij}=\xi_k[\epsilon_{ijk}Q_1+\epsilon_{ilk}(\delta_{lj}Q_2+\xi_jQ_3)] \tag{8}$$

where Q_1, Q_2, and Q_3 are arbitrary scalar functions of r^2 and μr, and ϵ_{ijk} is the alternating tensor. The relation between the skew axisymmetric tensor and the covariance tensor is:

$$\tilde{Q}_{ij}=\epsilon_{j\ell m}\frac{\partial\tilde{q}_{im}}{\partial\xi_\ell} \tag{9}$$

Since the axisymmetric tensor is symmetrical and solenoidal, it follows that

$$Q_3=\left(\frac{\partial}{\partial\xi_1}-\frac{\xi_1}{\xi_3}\frac{\partial}{\partial\xi_3}\right)Q_1 \tag{10}$$

Thus, the axisymmetric tensor can be defined by two scalars, Q_1 and Q_2. From Eqs. (8-10) the following tensor component relations were obtained by Goldstein and Rosenbaum[15]:

$$\tilde{Q}_{11}=-\frac{1}{\sigma}\frac{\partial}{\partial\sigma}(\sigma^2Q_1) \tag{11}$$

$$\tilde{Q}_{22}=-\frac{\partial}{\partial\xi_3}(\xi_3Q_2)+\left(\xi_3^2\frac{\partial^2}{\partial\xi_1^2}-2\frac{\partial^2}{\partial\xi_1\partial\xi_3}\xi_1\xi_3+\xi_1^2\frac{\partial^2}{\partial\xi_3^2}\right)Q_1 \tag{12}$$

$$\tilde{Q}_{33}=-\frac{\partial}{\partial\xi_2}(\xi_2Q_2)+\left(\xi_2^2\frac{\partial^2}{\partial\xi_1^2}-2\frac{\partial^2}{\partial\xi_1\partial\xi_2}\xi_1\xi_2+\xi_1^2\frac{\partial^2}{\partial\xi_2^2}\right)Q_1 \tag{13}$$

$$\tilde{Q}_{13}=\frac{\partial}{\partial\xi_1}(\xi_3Q_1) \tag{14}$$

$$\tilde{Q}_{12}=\frac{\partial}{\partial\xi_1}(\xi_2Q_1) \tag{15}$$

where

$$\sigma=\sqrt{\xi_2^2+\xi_3^2}$$

To implement this theory it becomes necessary to express the scalar functions, Q_1 and Q_2, in such a way that they include parameters related to measurable turbulence quantities. The cross-correlation coefficient $\tilde{R}_{ij}$ in the axisymmetric system has the general form of Eq. (1) and is based upon velocity components $\tilde{u}_i$ and $\tilde{u}_j$, with probe separation in terms of the movable probe position $(\tilde{r}_1,\tilde{r}_2)$. The relations between the correlation coefficient R_{ij} (measurement system) and that of $\tilde{R}_{ij}$ (axisymmetric system) are, assuming local

homogeneity:

$$\overline{u_1^2}R_{11}=\overline{\tilde{u}_1^2}\cos^2\phi\tilde{R}_{11}-2(\overline{\tilde{u}_1^2}\cdot\overline{\tilde{u}_2^2})^{1/2}\sin\phi\cos\phi\tilde{R}_{12}+\overline{\tilde{u}_2^2}\sin^2\phi\tilde{R}_{22} \quad (16)$$

$$\overline{u_2^2}R_{22}=\overline{\tilde{u}_1^2}\sin^2\phi\tilde{R}_{11}+2(\overline{\tilde{u}_1^2}\cdot\overline{\tilde{u}_2^2})^{1/2}\sin\phi\cos\phi\tilde{R}_{12}+\overline{\tilde{u}_2^2}\cos^2\phi\tilde{R}_{22} \quad (17)$$

$$(\overline{u_1^2u_2^2})^{1/2}R_{12}=(\overline{\tilde{u}_1^2}\tilde{R}_{11}-\overline{\tilde{u}_2^2}\tilde{R}_{22})\sin\phi\cos\phi+(\overline{\tilde{u}_1^2}-\overline{\tilde{u}_2^2})^{1/2}\cos2\phi\tilde{R}_{12} \quad (18)$$

for which the angular relations of the two reference frames are defined in Fig. 9.

IV. Theoretical Modeling and Experimental Comparisons

Goldstein and Rosenbaum Model

Goldstein and Rosenbaum[15] have chosen the following relations for the two defining scalars, Q_1 and Q_2,

$$Q_1(\xi_1,\sigma)=-\frac{\overline{\tilde{u}_1^2}}{2}\exp-\left[\left(\frac{\xi_1}{\ell_1}\right)^2+\left(\frac{\sigma}{\ell_2}\right)^2\right]^{1/2} \quad (19)$$

$$Q_2(\xi_1,\sigma)=-(\overline{\tilde{u}_2^2}-\overline{\tilde{u}_1^2})\exp-\left[\left(\frac{\xi_1}{\ell_1}\right)^2+\left(\frac{\sigma}{\ell_2}\right)^2\right]^{1/2} \quad (20)$$

In isotropic turbulence $\ell_1=\ell_2$ and $\overline{\tilde{u}_1^2}=\overline{\tilde{u}_2^2}$, which lead to $Q_2=0$, resulting in a single defining scalar function as expected. By using Eqs. (19) and (20), Eqs. (11-15) can be solved to get the correlation coefficients in the axisymmetric coordinates system, e.g.,

$$\tilde{R}_{11}=\left[1-(\sigma^2/2\ell_2^2)\left(\left(\frac{\xi_1}{\ell_1}\right)^2+\left(\frac{\sigma}{\ell_2}\right)^2\right)^{-1/2}\right]\times\exp-\sqrt{\left(\frac{\xi_1}{\ell_1}\right)^2+\left(\frac{\sigma}{\ell_2}\right)^2} \quad (21)$$

The parameters ℓ_1 and ℓ_2, were computed using the measured experimental length scales, defined by

$$L_{ii}^{\theta}=\int_0^{\infty}R_{ii}\left(\frac{Y}{R},r,\theta\right)dr \quad (22)$$

for different values of θ. For example, at $\theta=90$ deg, the parameter relations are

$$\left(\frac{\ell_1}{\ell_2}\right)^2=\frac{2\sin^2\phi\{[(\overline{\tilde{u}_1^2}/\overline{\tilde{u}_2^2})-1][(S+1)\cos^2\phi-1]+S\}}{1-2\cos^2\phi\{[(\overline{\tilde{u}_2^2}/\overline{\tilde{u}_1^2})-1][(S+1)\cos^2\phi-1]+S\}} \quad (23)$$

and

$$\ell_1=\frac{\overline{\tilde{u}_1^2}L_{22}^{\theta=90}[\sin^2\phi+(\ell_1/\ell_2)^2\cos^2\phi]^{1/2}}{\overline{\tilde{u}_1^2}\sin^2\phi+\overline{\tilde{u}_2^2}\cos^2\phi} \quad (24)$$

with

$$S=\frac{\overline{u_1^2}L_{11}^{\theta=90}}{\overline{u_2^2}L_{22}^{\theta=90}} \quad (25)$$

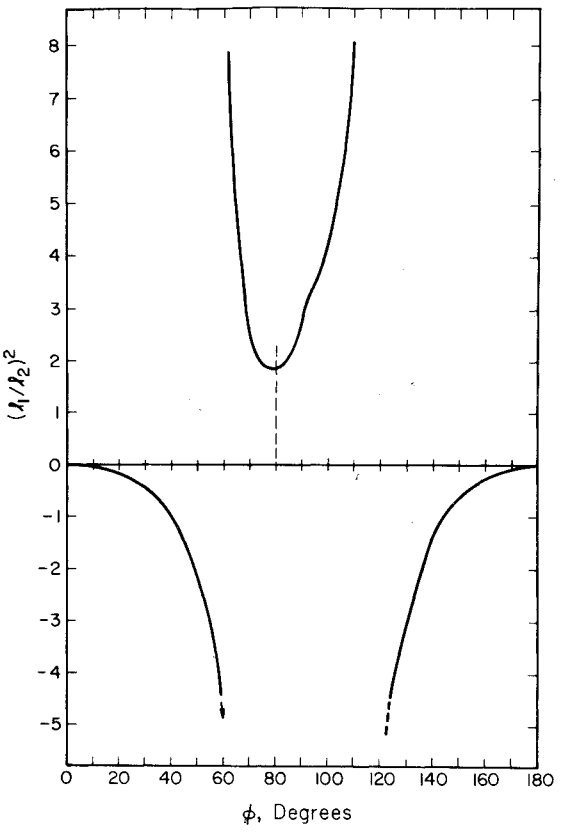

Fig. 10 Angular dependence of free parameter ratio in Goldstein and Rosenbaum[15] model.

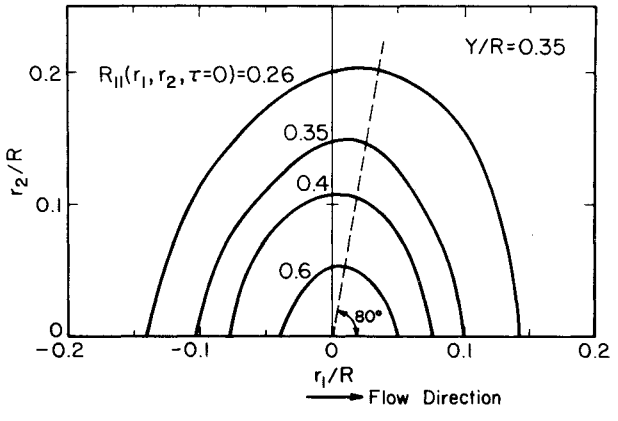

Fig. 11 Isocorrelation contours of R_{11} in Goldstein and Rosenbaum[15] model.

Using the proposed relations of Goldstein and Rosenbaum[15] and our measured experimental length scales, the allowed angles of axisymmetry led to unsuitable correlation coefficients which did not coincide with the observed angles of inclination of the isocorrelation contours. Figure 10 shows the relation between $(\ell_1/\ell_2)^2$ and the angle of axisymmetry ϕ evaluated from the available experimental data at position $Y/R=0.35$. This shows that the only available axisymmetric angles which give acceptable values of $(\ell_1/\ell_2)^2$ are for $\phi\sim80$ deg. The R_{11} and R_{22} isocorrelation contours computed by using $\phi=80$ deg are shown in Figs. 11 and 12, respectively. It is readily observed, when compared with isocorrelations obtained from the experimental data for pipe flow at $Y/R=0.35$, as shown in Figs. 6 and 7, that the model predictions are unacceptable. This suggests that further

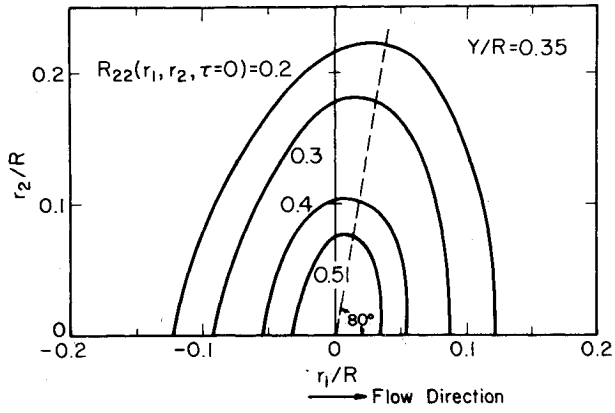

Fig. 12 Isocorrelation contours of R_{22} in Goldstein and Rosenbaum[15] model.

development is necessary to utilize the axisymmetric model for pipe flow turbulence.

Proposed Axisymmetric Model

The inability of the Goldstein and Rosenbaum[15] two-parameter model using two turbulence length scales to generate realistic correlation coefficients in turbulent pipe flow led to postulation of a more general axisymmetric model using four turbulence length scales to define the two scalar functions, Q_1 and Q_2. Two parameters, ℓ and n, are defined in terms of four turbulence related quantities, ℓ_1, ℓ_2, n_1, and n_2 as suggested by Weber[16] and for pipe flow applied initially by Cintra.[17] They are given in Cartesian coordinates by

$$\frac{r}{\ell}=\sqrt{\left(\frac{\xi_1}{\ell_1}\right)^2+\left(\frac{\xi_2}{\ell_2}\right)^2} \tag{26}$$

$$\frac{r}{n}=\sqrt{\left(\frac{\xi_1}{n_1}\right)^2+\left(\frac{\xi_2}{n_2}\right)^2} \tag{27}$$

and in polar coordinates by

$$\frac{1}{\ell}=\sqrt{\frac{\cos^2\beta}{\ell_1^2}+\frac{\sin^2\beta}{\ell_2^2}} \tag{28}$$

$$\frac{1}{n}=\sqrt{\frac{\cos^2\beta}{n_1^2}+\frac{\sin^2\beta}{n_2^2}} \tag{29}$$

These relations show that the two parameters, ℓ and n, have a constant value for constant angle β regardless the value of r.

The corresponding defining scalar Q_1, defined by Eq. (19), is unchanged for this four-parameter system. However, Q_2, defined in Eq. (20), has the argument of the exponential under the square root replaced by either Eq. (27) or (29), depending upon the coordinate system being used.

Thus, the correlation relations in the axisymmetric polar coordinate system become

$$\tilde{R}_{11}=\left(1-\frac{1}{2}\frac{r}{\ell_2^2}\frac{\sin^2\beta}{\sqrt{\frac{\cos^2\beta}{\ell_1^2}+\frac{\sin^2\beta}{\ell_2^2}}}\right)e^{-r/\ell} \tag{30}$$

$$\tilde{R}_{22}=\left(1-\frac{\overline{\tilde{u}_1^2}}{\overline{\tilde{u}_2^2}}\right)e^{-r/n}+\left(\frac{\overline{\tilde{u}_1^2}}{\overline{\tilde{u}_2^2}}\right)\times\left(1-\frac{1}{2}r\cos^2\beta\sqrt{\frac{\cos^2\beta}{\ell_1^2}+\frac{\sin^2\beta}{\ell_2^2}}\right)e^{-r/\ell} \tag{31}$$

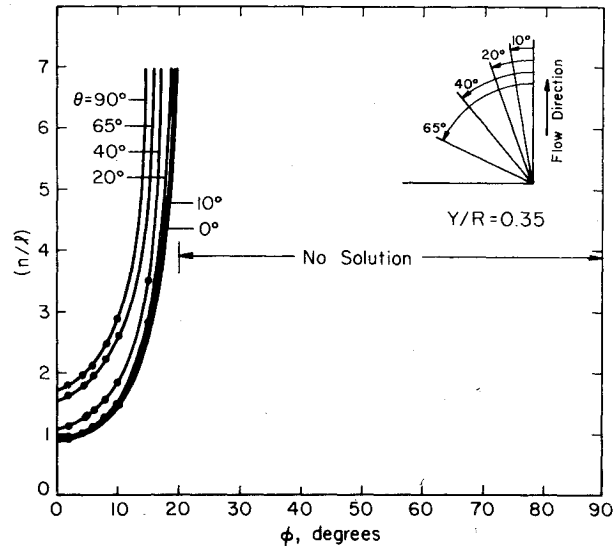

Fig. 13 Angular dependence of (n/ℓ) parameter ratio in proposed axisymmetric model.

$$\tilde{R}_{12}=\frac{1}{2}\left(\frac{\overline{\tilde{u}_1^2}}{\overline{\tilde{u}_2^2}}\right)^{1/2}\left(=\frac{r\sin\beta\cos\beta}{\ell_1^2\sqrt{\frac{\cos^2\beta}{\ell_1^2}+\frac{\sin^2\beta}{\ell_2^2}}}\right)e^{-r/\ell} \tag{32}$$

The four parameters, ℓ_1, ℓ_2, n_1, and n_2, have to be determined from the measured turbulence structure. It should be noted that the early attempt by Cintra[17] to introduce these four parameters was hampered by the lack of complete two-point x probe separation correlation data. In this study, since we have obtained a complete data set, these parameters can be determined from the experimental integral length scales at constant angle β through the following general relation

$$\tilde{L}_{ij}^{\beta}=\int_0^{\infty}\tilde{R}_{ij}(r,\beta)\,dr \tag{33}$$

in which ij can be 11, 22 and 12 or 21, and where $\tilde{L}_{ij}^{\beta}$ is the integral length scale in the axisymmetric coordinate system in the direction which makes an angle β with the ξ_1 axis (Fig. 9). By integrating Eq. (33) after substituting the correlation coefficients from Eqs. (30-32) we obtain, in the axisymmetric coordinate system,

$$\tilde{L}_{11}^{\beta}=\frac{1}{\sqrt{\frac{\cos^2\beta}{\ell_1^2}+\frac{\sin^2\beta}{\ell_2^2}}}\left[1-\frac{1}{2\ell_2^2}\frac{\sin^2\beta}{\left(\frac{\cos^2\beta}{\ell_1^2}+\frac{\sin^2\beta}{\ell_2^2}\right)}\right] \tag{34}$$

$$\tilde{L}_{22}^{\beta}=\left(1-\frac{\overline{\tilde{u}_1^2}}{\overline{\tilde{u}_2^2}}\right)\frac{1}{\sqrt{\frac{\cos^2\beta}{n_1^2}+\frac{\sin^2\beta}{n_2^2}}}+\frac{\overline{\tilde{u}_1^2}}{\overline{\tilde{u}_2^2}}\frac{1}{\sqrt{\frac{\cos^2\beta}{\ell_1^2}+\frac{\sin^2\beta}{\ell_2^2}}}\left(1-\frac{1}{2}\cos^2\beta\right) \tag{35}$$

$$\tilde{L}_{12}^{\beta}=\frac{1}{2}\left(\frac{\overline{\tilde{u}_1^2}}{\overline{\tilde{u}_2^2}}\right)^{1/2}\frac{\sin\beta\cos\beta}{\ell_1^2\left(\frac{\cos^2\beta}{\ell_1^2}+\frac{\sin^2\beta}{\ell_2^2}\right)^{3/2}} \tag{36}$$

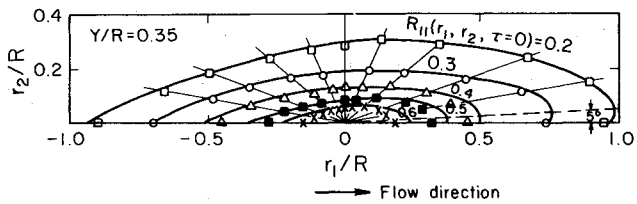

Fig. 14 Comparison of isocorrelation contours of $R_{11}(Y/R=0.35, r_1, r_2, \tau=0)$ in proposed axisymmetric model with experimental data.

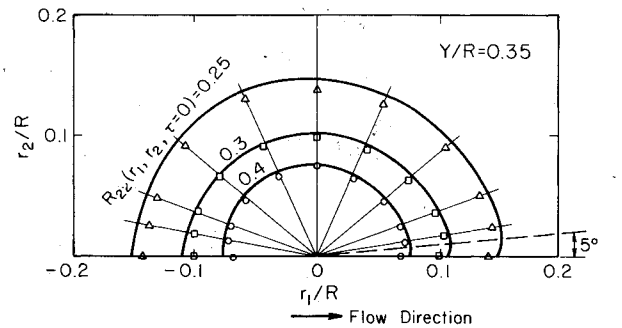

Fig. 15 Comparison of isocorrelation contours of $R_{22}(Y/R=0.35, r_1, r_2, \tau=0)$ in proposed axisymmetric model with experimental data.

If we set $\ell_1=\ell_2=\ell$ in Eq. (34), as for isotropic turbulence, we get

$$\tilde{L}^{\beta}_{11}=\ell(1-\tfrac{1}{2}\sin^2\beta)$$

which is similar to the results of Philip.[18]

The integral length scales in Eqs. (34-36) are related to the measured integral length scales through

$$\overline{u_1^2}L^{\theta}_{11}=\overline{\tilde{u}_1^2}\cos\phi\tilde{L}^{\beta}_{11}-2(\overline{\tilde{u}_1^2}-\overline{\tilde{u}_2^2})^{1/2}\sin\phi \cdot\cos\phi\tilde{L}^{\beta}_{12}+\overline{\tilde{u}_2^2}\sin^2\phi\tilde{L}^{\beta}_{11} \tag{37}$$

and

$$\overline{u_2^2}L^{\theta}_{22}=\overline{\tilde{u}_1^2}\sin^2\phi\tilde{L}^{\beta}_{11}+2(\overline{\tilde{u}_1^2}\cdot\overline{\tilde{u}_2^2})^{1/2}\sin\phi \cdot\cos\phi\tilde{L}^{\beta}_{12}+\overline{\tilde{u}_2^2}\cos^2\phi\tilde{L}^{\beta}_{22} \tag{38}$$

from which we can compute the parameters ℓ_1, ℓ_2, n_1, and n_2 by using data taken at two different angles of θ. These four nonlinear equations are solved using a standard subroutine.

Acceptable values for the parameter ratio n/ℓ, as shown in Fig. 13, were obtained only for small angles of ϕ, in agreement with experimental results. Figures 14 and 15 show the calculated correlation maps (as solid lines) for R_{11} and R_{22}, respectively, obtained from the axisymmetric model using the computed parameters $\ell_1=2.03$ cm, $\ell_2=1.73$ cm, $n_1=2.43$ cm, and $n_2=3.35$ cm, and the axisymmetric angle $\phi=5$ deg. These isocorrelation contours are compared with the experimental values obtained directly from Figs. 2 and 5 for R_{11} and R_{22}, respectively. The model is observed to predict satisfactorily the shapes of the measured contours. The averaged rms percentage differences between the measured correlation coefficients and those evaluated from the axisymmetric model for all 80 experimental separations in the r_1, r_2 plane for positive r_2/R were 16 and 11% for R_{11} and R_{22}, respectively. The largest percentage differences occur where the correlations are small, i.e., where the corresponding absolute differences are also small. Experimental confirmation was not obtained for negative values of r_2/R, e.g., approaching the wall. Because the axisymmetric model assumes homogeneity, we expect the strongly inhomogeneous wall region would not be as well represented by it.

V. Summary and Conclusions

This study has developed an axisymmetric turbulence model for modeling correlation coefficients in turbulent pipe flows. Cintra also found good agreement with the axisymmetric model at $Y/R=0.5$, suggesting that the model is a reasonable representation of the correlation structure in regions sufficiently far removed from the strongly inhomogeneous wall region in pipe flow. It has been compared with experimental measurements at $Y/R=0.35$ and shows good agreement with the measured correlation coefficients. In addition, the four integral length scales which were obtained from the space correlation data were found to exhibit a gradual change in relative values as the angle of probe separation increased from the mean flow direction.

From the measured data it was found that the isocorrelation contours of R_{22} were much less elongated and more nearly circular than those of R_{11} which suggests that the spatial extent of the coherent radial velocity fluctuations is much less than that of the axial velocity fluctuations.

References

[1] Favre, A., Gaviglio, J., and Dumas, R., "Space Time Double Correlations and Spectra in a Turbulent Boundary Layer," *Journal of Fluid Mechanics*, Vol. 2, 1957, pp. 313-342.

[2] Favre, A., Gaviglio, J., and Dumas, R., "Further Space Time Correlations of Velocity in a Turbulent Boundary Layer," *Journal of Fluid Mechanics*, Vol. 3, 1958, pp. 344-356.

[3] Davies, P.O.A.L. and Fisher, M. J., "The Characteristics of the Turbulence in the Mixing Region of a Round Jet," *Journal of Fluid Mechanics*, Vol. 15, 1963, pp. 337-367.

[4] Sabot, J. and Comte-Bellot, G., "Courves d'iso-correlations spatiales et d'iso-correlations spatio-temporelles relatives aux fluctuations longitudinales de vitesse en conduite lisse circulaire," C.R. Academy of Science, Paris, Vol. 275, Series A, 1972, pp. 667-670.

[5] Kovasznay, L.S.G., Kibens, V., and Blackwelder, R. F., "Large-Scale Motion in the Intermittent Region of a Turbulent Boundary Layer," *Journal of Fluid Mechanics*, Vol. 41, 1970, pp. 283-325.

[6] Batchelor, G. K., "The Theory of Axisymmetric Turbulence," *Proceedings of Royal Society*, Series A, Vol. 186, 1946, pp. 480-502.

[7] Chandrasekhar, F.R.S., "The Theory of Axisymmetric Turbulence," *Philosophical Transactions of Royal Society*, Series A, Vol. 242, 1950, pp. 557-577.

[8] Herring, J. R., "Approach of Axisymmetric Turbulence to Isotropy," *Physics of Fluids*, Vol. 17, No. 5, 1974, pp. 859-872.

[9] Sreenivasan, K. R. and Narasimha, N., "Rapid Distortion of Axisymmetric Turbulence," *Journal of Fluid Mechanics*, Vol. 84, No. 3, 1978, pp. 497-576.

[10] Burchill, W. E., "Statistical Properties of Velocity and Temperature Fields in Isothermal and Non-Isothermal Turbulent Pipe Flows," Ph.D. Thesis, Nuclear Engineering Program, Univ. of Illinois, 1970.

[11] Favre, A., "Review of Space Time Correlations in Turbulent Fluids," *Journal of Applied Mechanics, Transactions of ASME*, Vol. 32F, No. 241, 1965.

[12] Champagne, F. H., Harris, V. G., and Corrison, S., "Experiments on Nearly Homogeneous Turbulent Shear Flow," *Journal of Fluid Mechanics*, Vol. 41, No. 1, 1970, pp. 81-139.

[13] Mulhearn, P. J. and Luxton, R. E., "The Development of Turbulence Structure in a Uniform Shear Flow," *Journal of Fluid Mechanics*, Vol. 68, No. 3, 1975, pp. 577-590.

[14] Batchelor, G. K., *The Theory of Homogeneous Turbulence*, Cambridge University Press, England, 1967.

[15] Goldstein, M. and Rosenbaum, B., "Effect of Anisotropic Turbulence on Aerodynamic Noise," *Journal of Acoustical Society*, Vol. 54, No. 3, 1973, pp. 630-645.

[16] Weber, D. P., "Turbulent Velocity Field Structure in a Round Jet and Its Relation to Fluctuating Pressure," Ph.D. Thesis, Nuclear Engineering Program, Univ. of Illinois, 1974.

[17] Cintra, J.D.S., "Experimental and Modeling Studies of Two-Point Velocity and Temperature Fields in Turbulent Pipe Flow," Ph.D. Thesis, Nuclear Engineering Program, Univ. of Illinois, 1975.

[18] Philip, J. R., "Relation between Eulerian and Lagrangian Statistics," *The Physics of Fluids*, Supplement, 1967, pp. S68-S71.